Parametric plate-bridge dynamic filter model of violin radiativity

George Bissinger[a)]
East Carolina University, Greenville, North Carolina 27858

(Received 29 September 2011; revised 3 May 2012; accepted 3 May 2012)

A hybrid, deterministic-statistical, parametric "dynamic filter" model of the violin's radiativity profile [characterized by an averaged-over-sphere, mean-square radiativity $\langle R(\omega)^2\rangle$] is developed based on the premise that acoustic radiation depends on (1) how strongly it vibrates [characterized by the averaged-over-corpus, mean-square mobility $\langle Y(\omega)^2\rangle$] and (2) how effectively these vibrations are turned into sound, characterized by the radiation efficiency, which is proportional to $\langle R(\omega)^2\rangle/\langle Y(\omega)^2\rangle$. Two plate mode frequencies were used to compute 1st corpus bending mode frequencies using empirical trend lines; these corpus bending modes in turn drive cavity volume flows to excite the two lowest cavity modes A0 and A1. All widely-separated, strongly-radiating corpus and cavity modes in the low frequency deterministic region are then parameterized in a dual-Helmholtz resonator model. Mid-high frequency statistical regions are parameterized with the aid of a *distributed*-excitation statistical mobility function (*no* bridge) to help extract bridge filter effects associated with (a) bridge rocking mode frequency changes and (b) bridge-corpus interactions from 14-violin-average, excited-*via-bridge* $\langle Y(\omega)^2\rangle$ and $\langle R(\omega)^2\rangle$. Deterministic-statistical regions are rejoined at ~630 Hz in a mobility-radiativity "trough" where all violin quality classes had a common radiativity. Simulations indicate that typical plate tuning has a significantly weaker effect on radiativity profile *trends* than bridge tuning. © *2012 Acoustical Society of America*.
[http://dx.doi.org/10.1121/1.4726010]

PACS number(s): 43.75.De, 43.40.At, 43.40.Rj [JW] Pages: 465–476

I. INTRODUCTION

It is no simple matter to separate "great" violins from "good" ones by straightforward vibration or acoustic radiation measurements. At present this evaluation is best handled by the great violinists themselves. As a consequence a psychoacoustic curtain is drawn between the measurements (and physics) and the quality rating. No truly closed-form analytic model can pursue this issue. Mathematically intractable shapes, irreproducible materials, glue joints between porous materials, the violin bridge filter and its mode-specific interaction with the corpus (top+ribs+back), vibro-acoustic interactions between cavity air and corpus shell motions, and the conversion of mechanical energy to acoustic energy by a ported, doubly arched, nominally orthotropic composite shell structure only add to the formidable obstacles to constructing any comprehensive analytic model.

Yet the very consistency of certain legendary makers argues for them having some underlying "conceptual" system to navigate their way to a successful conclusion. Can we, centuries displaced from these makers and with no real evidentiary trail, while still respecting the underlying science of structural acoustics, gain some understanding of their thinking? Confining ourselves to traditional violins with tradition materials and shapes we start by assuming that only those violin substructures that makers commonly "tune" prior to sale, viz., the top and back plates (pre-assembly) and the bridge (post-assembly setup, *always* with sound post), are the most important determiners of violin sound. (Our presumption being that no business would take the time and effort to do something extra if it did not improve the sellability—the sound—of their product.)

Always staying within these boundaries we choose the radiativity $R(\omega)$, the complex frequency response function computed from the ratio of far-field microphone pressure response $P(\omega)$ (measured at 266 points over a sphere in an anechoic chamber) to the hammer-impact driving force $F(\omega)$ applied at the violin bridge corner, i.e., $P(\omega)/F(\omega)$ in Pa/N, as our basic measure of violin radiation. The violin's radiativity "profile" is then computed from the mean-square, average-over-sphere total radiativity $\langle R(\omega)^2\rangle$.

Our ultimate goal is to create a plausible "skeleton" radiativity profile filter model that captures the main structures of $\langle R(\omega)^2\rangle$ by choosing parameters that reflect comprehensive radiation and vibration experiments while still being consistent with general structural acoustics principles. In effect to *model the violin not by what it is, but by what it does*—a dynamic filter, as it were, interposed between driving force and sound, to examine *trends* based solely on *variations in plate and bridge tunings*.

II. DYNAMIC FILTER MODEL

The filter functions used in the model arise from the mathematical implementation of a simple concept expressed initially in the form of an identity. Because there is no theory capable of computing the radiativity profile starting with a force applied at the bridge, our approach is to let the violin "solve" this problem, then comprehensively measure dynamic

a)Author to whom correspondence should be addressed. Electronic mail: bissingerg@ecu.edu

responses and parameterize observed systematic behaviors in a way consistent with basic structural acoustics.

A. Fundamental premise

For a driving force applied at the bridge the fundamental premise of the dynamic filter model is that the sound radiation from the violin depends on two factors: (1) how vigorously it is vibrating, parameterized by $\langle v(\omega)^2\rangle$, the mean-square, surface-normal velocity averaged over the corpus, and (2) how effectively vibrational motions are converted to radiation, parameterized by $\langle P(\omega)^2\rangle$ the mean-square pressure averaged over a sphere, divided by $\langle v(\omega)^2\rangle$, both factors treated as "filters." This premise is expressed in the identity $\langle P(\omega)^2\rangle = \langle v(\omega)^2\rangle \cdot \{\langle P(\omega)^2\rangle / \langle v(\omega)^2\rangle\}$, a "cascade" of two filters whose product characterizes the violin's skeleton radiativity profile. To incorporate a mechanism for exciting the two lowest cavity modes, low frequency modes are modeled independently and reattached to the mid-high frequency region.

An equivalent identity that explicitly incorporates the driving force at the bridge involves the experimental modal analysis (EMA) mobility $Y(\omega)$, the complex frequency response function computed from $v(\omega)/F(\omega)$, which is used to compute a mean-square, averaged-over-corpus $\langle Y(\omega)^2\rangle$. [Our 17-violin radiativity database contains only 14 violins with $\langle R(\omega)^2\rangle$ and $\langle Y(\omega)^2\rangle$.] Hence $\langle R(\omega)^2\rangle = \langle Y(\omega)^2\rangle \cdot \{\langle R(\omega)^2\rangle / \langle Y(\omega)^2\rangle\}$.$\langle Y(\omega)^2\rangle$ deals only with the *vibrational* chain: string→bridge→corpus, while the $\langle R(\omega)^2\rangle / \langle Y(\omega)^2\rangle$ term deals only with the transformation of vibrational motion into acoustic radiation, embodied in the model by the dimensionless radiation efficiency $R_{eff}(\omega)$. [Henceforth for brevity frequency dependences for $P(\omega)$, $R(\omega)$, $v(\omega)$, $Y(\omega)$ and $R_{eff}(\omega)$ can always be understood.]

Our unique experimental circumstance—a driving force applied at the bridge (zero-mass-loading so as not to affect the bridge rocking frequency) that is common to *simultaneous* mobility and radiativity response measurements on a violin suspended "free-free" in an anechoic chamber—makes $\langle R^2\rangle / \langle Y^2\rangle$ a reliable substitute for $\langle P^2\rangle / \langle v^2\rangle$. Driving forces applied at the bridge necessarily incorporate bridge "filter" effects including: (a) bridge rocking frequency f_{rock} (where f_{rock} is normally measured with the bridge feet clamped in a vise) and (b) the interaction of the bridge feet with the top plate in the "bridge island" region.

The defining equation for the dynamic filter model now becomes

$$\langle R^2\rangle = \langle Y^2\rangle \frac{\langle P^2\rangle}{\langle v^2\rangle}, \tag{1}$$

where $\langle P^2\rangle / \langle v^2\rangle$, calculated from $\langle R^2\rangle / \langle Y^2\rangle$, contains the dynamics needed to compute R_{eff}.

B. Deterministic-statistical division

Cremer in 1984 suggested[1] "there is a range of low frequencies in which easily separable natural frequencies can be examined deterministically"—our signature mode region—"and a higher one at which only statistical statements are possible in the frequency domain," the latter where modes overlap significantly, mode tracking becomes problematical, and statistical band-averages over multiple modes become more suitable. Our hybrid dynamic filter model is based on just such a scheme. These distinct regions are separated in the violin by a broad, relatively featureless mobility-radiativity "trough" transition region from ~600 to ~750 Hz that features a key experimental finding, viz., at ~630 Hz the *f*-hole, surface and background radiativity contributions sum to $\langle R\rangle \approx 0.19$ Pa/N, irrespective of violin quality class, to provide a crucial splice point for the independent deterministic and statistical regions.

In the proposed deterministic region below 600 Hz five well-separated "signature" modes appear: the two coupled lowest cavity modes A0 and A1 ($f_{A0} \approx 275$ Hz, $f_{A1} \approx 465$ Hz), and three "corpus" modes: CBR near 400 Hz and the violin's 1st corpus bending modes $B1^-$ and $B1^+$ with $f_{B1^-} \approx 470$ Hz and $f_{B1^+} \approx 540$ Hz. A0, $B1^-$ and $B1^+$ are *always* strong radiators, while A1 radiation varies over a surprisingly wide range. CBR generally radiates so weakly that it will be ignored. These signature modes, suitably shifted in frequency, were also seen across the entire violin octet,[2] arguing for great generality in this choice of modes for the deterministic region. The bridge motions in these two regions were also dissimilar: in the deterministic region the bridge rocked approximately as a rigid body, while in the statistical region bridge motions can be characterized as quiet-feet/rocking-wiggling top.[3]

Some important experimental correlations needed in the model have no strong theoretical base, e.g., (1) an empirical trend line linkage between the frequencies (in the common labeling scheme) of violin plate modes #2 and #5, f_2 and f_5 (where f_2 is approximately one-half f_5) and the B1 modes provides an essential computational path[4] from f_2,$f_5 \leftrightarrow B1^-$,$B1^+$, and (2) a companion empirical trendline (shown later) linking f_5 to an *effective* critical frequency for the violin. [Note that a similarly important empirical relationship,[5] $1.5 \times f_5$, was used in Schelleng's flat-plate scaling scheme[6] to successfully place the "main wood" resonance (now the B1 modes) near the pitch of the upper middle string across the entire $3^1/_2$ octave range of the violin octet.]

In the statistical region 250 Hz band-averages were used to examine systematic modal-average behavior vs band center frequency f_c. To help isolate bridge filter effects a statistical mobility for *distributed* (e.g., roving hammer strikes over corpus, acoustic excitation, etc.) excitation of the violin was used in conjunction with experimental 14-violin *bridge*-excitation average mobility to back out a bridge filter function. A separate function based on systematic measurements accompanying bridge waist-wing trims was used to simulate the effect of bridge "tuning."

III. DETERMINISTIC REGION

The complexity of the signature mode region has been appreciated for quite a while. An important clarification of their interactivity came in an experiment by Weinreich, Holmes and Mellody[7] (WHM) who examined wood and cavity air motions driven by acoustic excitation as one or more

corks were removed from 42 holes drilled in the ribs of the "swiss-cheese" violin of Hutchins.[8] They concluded that the experimentally observed interaction between A0, A1 and the B1 modes could be modeled by incorporating coupling in a "dynamic modes" theoretical approach to the coupled vibrations of fluids and enclosures. Based on (1) the conclusions of Weinreich *et al*., (2) a range of prior experimental data, *plus* (3) two additional experimental results presented below that support the sound hole sum rule of Weinreich,[9] the assumption that A0 excitation is driven by B1 wall motions alone is the basis of our deterministic region model.

A. A0 excitation

A0, the only always-strongly-radiating mode in the violin's lowest octave, has long been understood as being particularly important to violin sound. Moreover, of 17 violins in our radiativity database the only statistically important difference between bad and excellent violins was A0 radiativity $\langle R_{A0}\rangle$.[10] (Note that three violins had partial or nonexistent mobility scans, hence no R_{eff} calculations were possible.) Any reasonably complete model of the violin's radiativity profile requires a plausible model for A0 excitation that reflects extensive experimental results:

(1) $\langle R_{A0}\rangle$ decreased as the A0-B1$^-$ frequency difference Δf increased.[11]
(2) Sound post removal drops f_{A0} by ~30 Hz and R_{A0} greatly decreases.[12,13] EMA results show sound post removal also eliminated a B1$^-$-*like* mode while a B1$^+$-*like* mode dropped approximately 50 Hz.[13]
(3) Below 700 Hz, B1$^-$ and B1$^+$ show large volume changes in the $\lambda >$ largest-dimension region, with large *in*-phase inter-*f*-hole, *in*-phase volume flows (like A0) comparable to EMA-based estimates of volume changes.[14]
(4) Varying the bridge's 1st rocking mode frequency f_{rock}—measured with both feet clamped in a heavy vise—revealed that mobility-radiativity data for one modern and one old Italian violin exhibited ~1:1 correlation between R_{A0} and B1 mode excitation represented by average bridge foot mobility $\langle Y_{bf}\rangle$ as seen in Fig. 1.

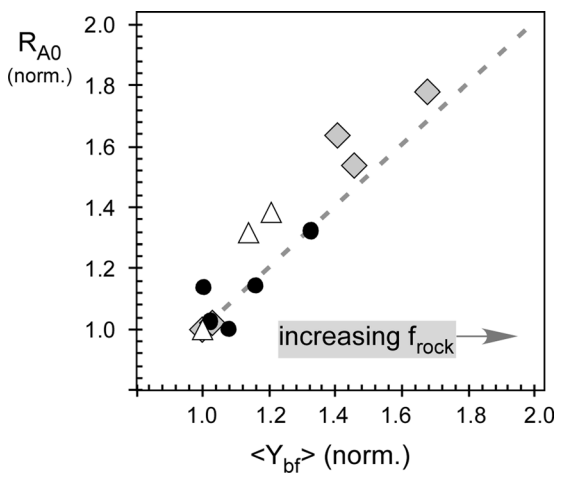

FIG. 1. R_{A0} vs average B1 bridge foot mobility $\langle Y_{bf}\rangle$ for two violins (both norm. to lowest value) as f_{rock} varied. 2004 dataset (2.8–3.6 kHz: A. Guarneri (1660) •; G. Alf ◇ (2003) and 2005 dataset (2.6–3.4 kHz: A. Guarneri △). (Dashed line represents 1:1 correlation to guide eye.)

(5) From ~0.7 to ~2 kHz, f_{rock} changes had little or no effect on corpus mode excitation, hence these modes cannot be important for A0 excitation. Above 2 kHz f_{rock} changes showed the maximum effect on radiativity at frequencies near f_{rock} that were *much* larger proportionately than the effect on R_{A0}[3]; this lack of ~1:1 correlation implies that modes above 2 kHz cannot be important for A0 excitation. (Further discussion on this matter in statistical region model.)
(6) R_{A0} was observed to correlate ~1:1 with *changes* in B1 radiativity R_{B1} in an Oberlin Violin Acoustics Workshop experiment where sound post *diameter* was trimmed in successive stages on three violins (f_{A0}, f_{B1} and associated dampings remained unchanged). The results, shown in Fig. 2 for the first time, have B1 excitation varying in a non-systematic way between violins, but R_{A0} always followed the B1 variations.

The results in Figs. 1 and 2 reflect the fundamental A0-B1 linkage in the sound hole sum rule as expressed by Weinreich in his response to a violinmaker about what to do to increase A0 radiativity: "the somewhat surprising answer is, 'nothing'. Because of the Sound Hole Sum Rule… one cannot raise the Helmholtz mode without increasing the following modes equally."[15] Taking all these results together we henceforth assume that R_{A0} directly correlates 1:1 *only* with B1 excitation/radiativity.

Since a B1-wall-driven, dual-Helmholtz resonator network model *automatically* correlates $\langle R_{A0}\rangle$ with R_{B1} *f*-hole radiativity (the dominant radiative path) in accord with experiment (Figs. 1 and 2) we choose to employ this model, acknowledging its formal weaknesses while recognizing that it offers a convenient *formalism* to compute total radiativity in a parametric model that adds B1 surface and higher mode background contributions to compute $\langle R\rangle$ for all the strongly radiating signature modes.

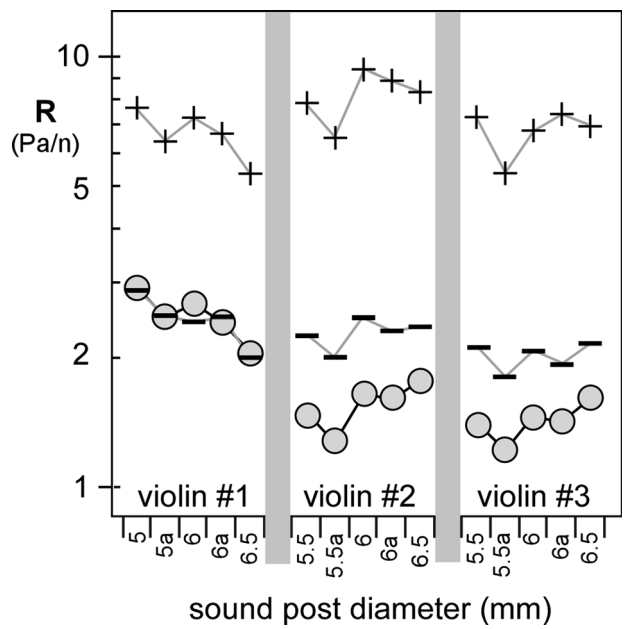

FIG. 2. (log) R_{A0} (○), B1$^-$ (−) and B1$^+$ (+) radiativity at 0.3 m vs sound post diameter trims from 6.5 to 5 or 5.5 mm on three violins.

1. A0-A1 network model

Our model is similar in concept to a successful 1980 Christensen and Vistisen model of low-frequency guitar sound based on a coupling between the lowest corpus mode—a (mostly) top plate mode that acted like a piston—and the Helmholtz cavity resonance.[16] A1, due to its coupling to A0 and strong effect on A0 volume dependence in the violin, was also incorporated, following the 1990 network model of Shaw.[17] The A0-A1 coupling inherent in the Shaw model brings the predicted A0 volume dependence for a rigid violin-shaped cavity in line with experiment.[18] Our parametric model preserves such essentials of the Shaw model as two partial volumes connected by a constricted (pipe) region to incorporate A0 and A1, but does not incorporate the Shaw division parameters α (the fraction of C-bout inertance above the *f*-hole center point) and β (fraction of *f*-hole inertance in lower bout volume) in order to retain the simplicity inherent to a Helmholtz resonator network model for *f*-hole radiativity computations.

To understand A1 variability in this model consider a slightly flexible bottle attached neck-to-neck to a similar but somewhat smaller bottle, with a port drilled somewhere in the combined neck. (Cf., "one can think of the A1 as a mode of two Helmholtz resonators attached mouth to mouth."[7]) The smaller bottle corresponds to the upper bout (UB), the larger bottle to the lower bout (LB) and the neck plus port to the intermediate waist C-bout (CB) region of the violin with *f*-holes. If the bottles are compressed in-phase, air would be expelled through the port. If the bottles are compressed antiphase a "slosh" motion of the interior air would result, with negligible port air flow. Suppose further that initially *only one bottle was compressed*, creating compress *and* slosh air motions; the other bottle then being compressed in-phase, weakly at first, and then increasingly strongly. At some point the oppositely directed slosh flows associated with each partial volume compression will just cancel out, leaving only compress flows through the *f*-holes. Thus *slosh flows*—and A1 excitation—*arise naturally from an imbalance between UB-LB cavity volume flows*. Lack of slosh flow implies *no* A1 excitation-radiation.

Such a *dual*-Helmholtz resonator with compress and slosh cavity volume flows corresponding to A0 and A1, resp., comprises our physical model for A0 and A1 excitation driven by B1 corpus wall motions. Melding two single-cavity networks[19] produces the network shown in Fig. 3. The nominal violin total volume V is fixed at 2000 cm^3, but

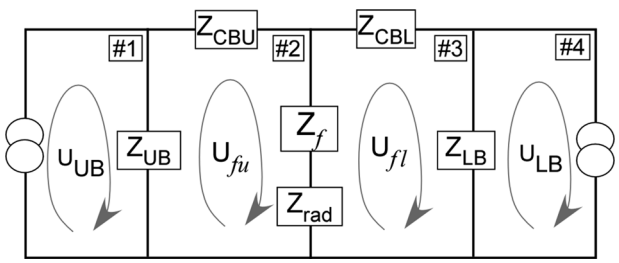

FIG. 3. Dual Helmholtz resonator network with relevant impedances, volume flows, and loops (standardized cavity volume flow direction, loops numbered for later reference).

apportioned into partial volumes, initially using optimized rigid cavity Shaw model network values.[18] Acoustic impedances were computed from standard Helmholtz resonator equations:[19] UB, LB cavity volumes V_{UB} and V_{LB} used $Z_{cav} \approx j\rho c^2/V\omega$; pipe equations used $Z_{pipe} \approx j\omega\ (\rho l/S)$; pipe lengths $= l$, cross section area $= S$. CB waist area at bridge $= S_{CB}$, length $= l_{cb} \approx 15$ cm, broken into two parts l_{cbu} and l_{cbl} that sum to l_{cb}. Port (*f*-hole) area $S_f \approx 12$ cm^2, and $l_f \approx 0.8$ cm. The port radiation impedance $Z_{rad} \approx 0.16\rho\omega^2/c + 0.6\ j\omega\rho a/S_f$; port radius/area ratio in 2nd term of Z_{rad} computed from nominal circle-equivalent area $S_f = \pi a^2$, fixed for all calculations. Additionally, resistive damping was added to Z_{rad} to achieve measured A0 total damping $\zeta \approx 2.5$ (in %-of-critical, $Q \approx 20$); A1 also incorporated resistive damping terms in the Z_{CB} impedances, adjusted to return experimental A1 damping of ~1%crit. Additional parameter values provided for a specific violin later.

B1 wall-motion-forced cavity volume flows U_{UB} and U_{LB} drive the net *f*-hole volume flow, $U_f = U_{fu} - U_{fl}$, seen in Fig. 3 (minus sign from standardized loop direction). UB and LB pressures, p_{UB}, p_{LB}, respectively, computed from the model were generally much larger for A1 than A0, and were reflected in their relative measured wall motions.

The network in Fig. 3 generated the following loop equations:

$$\#1:\ (U_{UB} - U_{fu})Z_{UB} = p_{ub}, \tag{2}$$

$$\#2:\ (U_{fu} - U_{UB})Z_{UB} + U_{fu}Z_{CBU} + U_f(Z_{rad} + Z_f) = 0, \tag{3}$$

$$\#3:\ (U_{fl} - U_{LB})Z_{LB} + U_{fl}Z_{CBL} - U_f(Z_{rad} + Z_f) = 0, \tag{4}$$

$$\#4:\ (U_{LB} - U_{fl})Z_{LB} = p_{lb}. \tag{5}$$

With solution

$$\begin{aligned} U_f = \{&(Z_f Z_{UB} U_{UB} + Z_{LB} Z_{UB} U_{UB} + Z_{CBL} Z_{UB} U_{UB} \\ &+ Z_{rad} Z_{UB} U_{UB} + Z_{LB} Z_{rad} U_{LB} + Z_{LB} Z_f U_{LB}) \\ &- (Z_{rad} Z_{UB} U_{UB} + Z_{LB} Z_{rad} U_{LB} + Z_{UB} Z_{LB} U_{LB} \\ &+ Z_f Z_{UB} U_{UB} + Z_{LB} Z_f U_{LB} + Z_{CBU} Z_{LB} U_{LB})\}/D, \end{aligned} \tag{6}$$

where

$$\begin{aligned} D = &Z_{LB} Z_{UB} + Z_{rad} Z_{UB} + Z_f Z_{CBU} + Z_f Z_{UB} + Z_{LB} Z_{rad} \\ &+ Z_{LB} Z_f + Z_{LB} Z_{CBU} + Z_{CBL} Z_f + Z_{CBL} Z_{CBU} \\ &+ Z_{CBL} Z_{UB} + Z_{rad} Z_{CBU} + Z_{CBL} Z_{rad}. \end{aligned} \tag{7}$$

U_{UB} and U_{LB} used a complex resonance wall-motion mobility equation of the form $\omega/[j(\omega^2 - \omega_{B1}{}^2) + \omega\omega_{B1}/Q_{B1}]$ for each B1. The in-phase cavity volume flows create the deep radiativity minimum seen between B1 modes. Given the net *f*-hole volume flow the power radiated through the port was computed from $\frac{1}{2}\mathrm{Re}(Z_{rad})U_f^2$, where $\mathrm{Re}(Z_{rad}) = 0.16\rho\omega^2/c$.

2. Surface and background contributions

In 2007 a "patch" near-field acoustical holography (pNAH) experiment on a Strad copy violin[14] demonstrated

that B1 mode *f*-hole radiativity R_f exceeded surface radiativity. For $B1^-$ and $B1^+$ total radiativity, $R_f = 0.67\langle R_{B1^-}\rangle$ and $0.56\langle R_{B1^+}\rangle$, hence B1 *surface-only* radiation can be computed from the difference $\langle R_{B1}\rangle - R_f$. (A1-*induced* surface motion from cavity volume flows cannot be computed in this model, although variability in A1 radiativity can be understood.)

Except for this one violin all simulations used $R_f \approx 0.6\langle R_{B1}\rangle$ for both B1. The nominal 40% corpus surface contribution was incorporated into total B1 radiativity by adding a resonant surface radiativity component R_{surf} based on the same B1 frequency-damping values used for R_f calculations, always adjusted to keep $R_{surf}/R_f = 0.67$. The conglomerated response tail for all modes above the signature modes was accounted for by adding a nominal background contribution $R_{bgd} \propto f$, constrained to give total radiativity $\langle R\rangle = R_f + R_{surf} + R_{bgd} \approx 0.19$ Pa/N at 630 Hz.

3. Strad copy simulation

The optimized A0-A1 rigid cavity network model[17] provided initial partial volumes and pipe lengths that were then adjusted slightly to return $f_{A0} = 275$ Hz and $f_{A1} = 453$ Hz for the Strad copy violin: volumes (cm^3) $V = 2000$ (fixed), $V_{UB} = 672$, $V_{LB} = 850$; areas (cm^2) $S_{CB} = 50$, $S_f = 12$ (both fixed); lengths (cm) $l_{cbu} = 12.2$, $l_{cbl} = 7.4$, $l_{cb} = 19.6$, $l_f = 0.80$; $R_f = 0.67\langle R\rangle$ and $0.56\langle R\rangle$ for $B1^-$ and $B1^+$, resp. Using $f_{B1^-} = 489$ Hz, $\zeta_{B1^-} = 1.2\%$crit, $f_{B1^+} = 515$ Hz, $\zeta_{B1^+} = 1.1\%$crit, R_{A0} was computed after adjusting U_{UB} and U_{LB} to achieve experimental radiativity values $R_{B1^-} = 0.72$ Pa/N and $R_{B1^+} = 0.84$ Pa/N. Comparisons between experiment and model simulations for R_{A0} are shown in Fig. 4 (statistical region discussed later) to validate the model, Estimating R_{A0} *trends* as B1 properties change is now quite straightforward.

B. R_{A0} dependence on B1 parameters

Using our 14-violin average $f_{A0} = 275$ Hz and $f_{A1} = 469$ Hz, the systematic dependence of *relative* A0 radiativity R_{A0} (rel.) on B1 frequencies (B1 radiativity fixed) was examined. Calculations of R_{A0} (rel.) were performed over a range of 430–510 Hz for the lower B1 mode for three cases: (1) only one B1, (2) two B1 with *fixed frequency difference* = 70 Hz, and (3) two B1 with *average frequency* = 505 Hz (one B1 drops while the other rises in frequency). Results are presented in Fig. 5.

The strong correlation between A0-B1 Δf and R_{A0} (rel.) in Fig. 5 mirrors that seen experimentally.[11] Pertinent to the effect of sound post removal, note that having *two* B1 modes greatly strengthens R_{A0} (rel.). The constant-average/rising-Δf between two B1 modes results in a significantly slower decrease in R_{A0} (rel.) than the rising-average/fixed-70 Hz Δf. Larger f_5/f_2 ratios were also observed to correlate with a greater spread in B1frequencies.[4]

1. Additional predictions for R_{A0}

Experimental and predicted values of $\langle R_{A0}\rangle$ were ~0.80 Pa/N for the smallest A0-$B1^-$ Δf. At the other extreme the Strad copy violin of Fig. 4 with almost the largest Δf gave $\langle R_{A0}\rangle \approx 0.33$ Pa/N, vs the experimental 0.29 Pa/N.

To properly interpret the effects of sound post removal on R_{A0} requires prior EMA results, viz., f_{A0} dropped approximately 30 Hz, the $B1^-$-like mode disappeared, a $B1^+$-like mode dropped ~50 Hz. *Pre*-removal $f_{B1^-} = 470$ Hz and $f_{B1^+} = 540$ Hz leads to an initial two-B1 estimate (interpolated to bypass A1 interference) of R_{A0} (rel.) ≈ 1.7. *Post*-removal (following the zigzag line in Fig. 5) there is only one $B1^+$-like mode at 490 Hz and R_{A0} (rel.) = 0.31, indicating a drop-off of ~5.4. Since f_{A0} dropped from 275 to 245 Hz, creating an additional ~30% drop-off, R_{A0} should fall by a factor of ~7 overall, consistent with that seen by Meinel.[12]

2. Predictions for A1 excitation

(1) A1 had $R_f \approx 0$ as expected for a cavity mode with a pressure node at the *f*-holes

(2) p_{ub} and p_{lb} depend strongly on U_{UB}/U_{LB}: $U_{UB}/U_{LB} < 0.7$ or > 1.1 gave A1 pressures ~10× A0, consistent with observed A0-A1 relative induced surface motions.

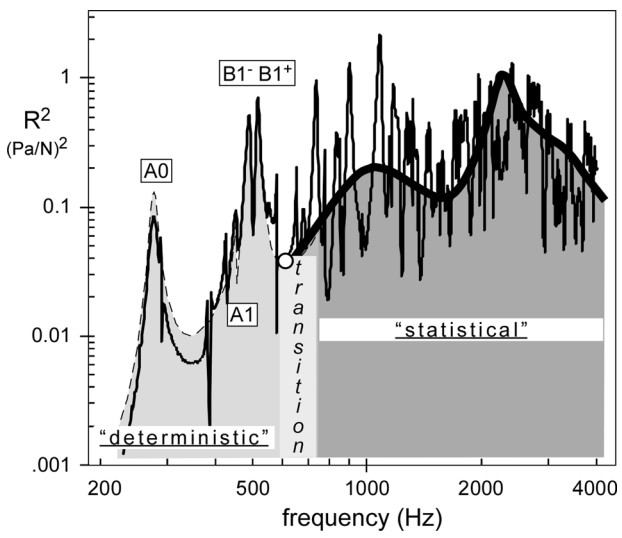

FIG. 4. Deterministic region: experimental $\langle R^2\rangle$ for Strad copy violin (thin line) vs dual-Helmholtz model (- -, light shade) norm. at 630 Hz (○). Statistical region (▬, thick line, darker shade) with $f_{rock} \approx 2.8$ kHz also shown (see text).

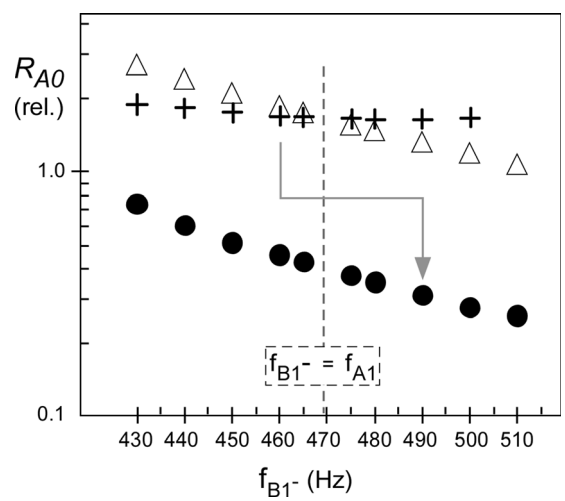

FIG. 5. Dual-Helmholtz model R_{A0} (rel.) for A0 at 275 Hz driven by: one-B1 (•), two-B1 with fixed Δf = 70 Hz (△), and two-B1 with 505 Hz average frequency (+). Gray zig-zag line represents sound post removal (see text).

(3) An A1 pressure null resulted for $U_{UB}/U_{LB} \approx 0.92$, suggesting little induced surface motion and hence little A1 radiation.
(4) When $f_{A1} \approx f_{B1}-$ A1 pressures increase. Since the lower bout has greater area and compliance than the upper bout, greater internal pressures over a larger, more compliant area imply a weak-dipole/dominant-monopole aspect to A1 surface mobility, seen most prominently in the *Plowden* del Gesu violin,[10] which had $\langle R_{A1}\rangle \approx \langle R_{B1-}\rangle$.
(5) If arch and rib height are varied:
   (a) *fixed-rib-height/increased-arching* increases violin volume *and* the C-bout cross-section area; net result - f_{A0} falls with increased arching while f_{A1} rises.
   (b) *fixed-arching/increased-rib-height*; net result - f_{A0} decreases, f_{A1} hardly changes.

In summary the dual-Helmholtz network model provides systematic R_{A0} predictions in agreement with a broad range of experiment when B1 radiativity and frequency-damping information is available for a particular violin. However it is really more appropriate for computing radiativity profile *trends* when B1 f, ζ and $\langle R_{B1}\rangle$ starting values are available and then varying plate and bridge tuning, the next step in the model.

IV. STATISTICAL REGION

The defining equation for the dynamic filter model, Eq. (1), where $\langle P^2\rangle/\langle v^2\rangle$ was computed from $\langle R^2\rangle/\langle Y^2\rangle$ contains all the dynamics needed to compute the radiation efficiency, viz., $R_{eff} = \langle R^2\rangle/\langle Y^2\rangle \cdot (A/\rho^2{}_o c^2 S)$ (A = microphone-sphere area = 18.1 m^2 and S = violin surface area = 0.13 m^2), hence

$$\langle R^2\rangle \propto \langle Y^2\rangle \cdot R_{eff}. \tag{8}$$

The first term on the RHS deals with corpus vibrational motion gained from a driving force applied at the bridge, while the 2nd term deals with how effectively the vibrational motion is transformed to acoustic radiation. These two terms act as independent filter functions, the string→bridge→corpus "gatekeeper" (so labeled because the bridge is such a strong filter for string energy on its way through to the corpus) and the R_{eff} "egress"; neither term has any specific violin shape or material parameters, all of which have been subsumed into the measured dynamics.

A. Damping—the "egress" filter

To put the simpler egress filter into a damping context for loss calculations, the violin is treated as a "leaky bucket" with three possible loss paths, viz., radiation, internal (heat) and support fixture damping. The total damping ζ_{tot} sums these, i.e., $\zeta_{tot} = \zeta_{rad} + \zeta_{int} + \zeta_{fix}$; ζ_{tot} was taken from mobility spectra fits (in %crit), ζ_{rad} was computed directly from R_{eff}, and $\zeta_{fix} \approx 0$ (effectively eliminated by our "free-free" support system), thus $\zeta_{tot} \approx \zeta_{rad} + \zeta_{int}$. To parameterize the total damping a simple, reliable ($r > 0.9$) power-law fit to the ζ_{tot} data, $\zeta_{tot} \propto f^{-0.34}$, was chosen for use throughout our analysis, rather than presuming some functional dependence for ζ_{int}.[11] (Again, all damping frequency dependence is understood.)

The simultaneous R and Y measurements led to an *effective* critical frequency for the violin,[10] utilized here in a "stylized" way to represent R_{eff} behavior (guided by the baffled piston's pressure dependence on velocity, viz., $P \propto fv$): $R_{eff} \propto f^2$ up to f_{crit}, where the dispersive flexural wave velocity v_{flex}, which rises as $f^{1/2}$, finally catches up with the speed of sound in air c. At $v_{flex} = c$, the $R_{eff} = 1$ plateau is reached, and maintained for $f \geq f_{crit}$.

This stylized R_{eff} behavior is subsequently reflected in the radiation damping, $\zeta_{rad}(\%crit) = R_{eff} \cdot (50\rho_o cS/2\pi Mf) \propto R_{eff}/fM$: $\zeta_{rad} \propto f$ for $f < f_{crit}$; for $f > f_{crit}$, $\zeta_{rad} \propto f^{-1}$, thus creating a "peak" in ζ_{rad}. Introducing the fraction of corpus vibrational energy radiated, $F_{RAD} = \zeta_{rad}/\zeta_{tot}$, into the egress leads to $R_{eff} \propto f\,M\,\zeta_{tot}\,F_{RAD}$.

The egress filter always peaks at f_{crit} because ζ_{tot} falls off smoothly, thus ζ_{rad} peaks at f_{crit}, as does F_{RAD}. To improve agreement with experiment a constant term was added to ζ_{rad} below f_{crit}, while above f_{crit}, F_{RAD} drop off was modified slightly to improve agreement with the overall radiativity profile. After substitution and rearrangement Eq. (8) becomes

$$\langle R^2\rangle \propto \{1/2\ M\langle Y^2\rangle\} \cdot \{f\xi_{tot}F_{RAD}\}. \tag{9}$$

Violin total mass M now appears naturally. The gatekeeper has become the driving-force-normalized kinetic energy, although its blandness cloaks a starkly different reality.

1. f_{crit} from arched plate f_5

The violin's slotted, doubly-arched, nominally orthotropic, relatively shallow shell defies easy theoretical analysis in computing a key parameter in the dynamic filter model, f_{crit}. Accordingly, rectangular flat plate theory, where $f_{crit} = c^2[12(1-\nu^2)\rho/E]^{1/2}/h \propto f_{bend}{}^{-1}$ (f_{bend} = bending mode frequency $\propto 1/h$, h = plate thickness, ν = Poisson's ratio, ρ = density, E = Young's modulus) suggests an alternative approach, a power law trend line linking f_{crit} and f_{bend}.

Flat plate theory predicts f_{crit} values for nominal violin plate thicknesses between 4 and 5 kHz for the along-grain propagation and 9–17 kHz for cross-grain propagation for the maple back and spruce top plate, respectively.[1] The along-grain values compare well with our 14-violin average effective $f_{crit} \approx 3.9$ kHz. The very high cross-grain (mode #2-like) critical frequency implies very low R_{eff} at lower frequencies and as a consequence little contribution to the overall radiation, which is predominantly into the top plate hemisphere at higher frequencies.

Some insight into shell membrane strain effects on the critical frequency can be gotten by rewriting a shell equation[19] $f_{mn} = (A_{mn} + B_{mn}h^2)^{1/2}$ as $f_5 = (A + Bh^2)^{1/2}$ and evaluating the A and B coefficients using a systematic plate thinning experiment,[20] giving $A^{1/2} \approx 200$ and $B^{1/2} \approx 80$ (h in mm). (For f_2, A ≈ 0.) Hence the suggestive rewriting, $f_5{}^2 = A + Bh^2 = f_{memb}{}^2 + f_{bend}{}^2$, leads to $f_{bend} \approx (f_5{}^2 - 40\,000)^{1/2}$. For a nominal $f_5 = 350$ Hz, $f_{bend} \approx 276$ Hz, an approx. 20% reduction. However since the flexural wave velocity $v_{flex} \propto f^{1/2}$, recomputing f_{crit} from $f_{crit} \approx (c/v_{flex})^2\, f_{bend} \approx (c/L)^2/f_5$[11] leads to an ~20% increase in f_{crit}. As f_5 decreases, leading to a proportionately larger membrane component, f_{crit} increases even more *relative to the flat plate* prediction. Expressing plate

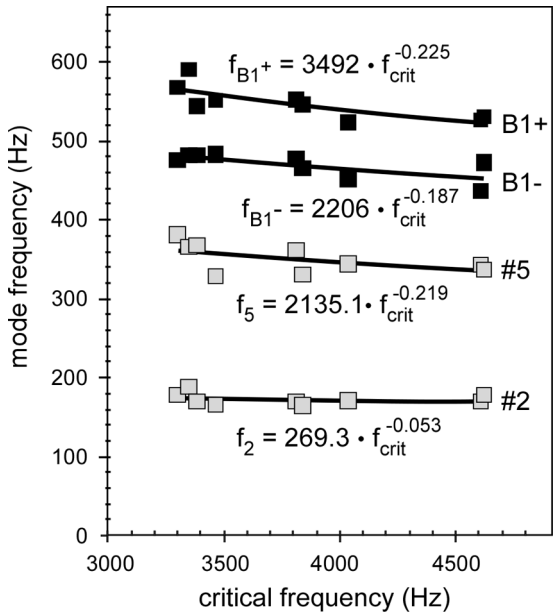

FIG. 6. Plate f_2, f_5 and corpus f_{B1^-} and f_{B1^+} vs effective f_{crit} for nine violins, with power-law trend line equations (f_{crit} in Hz).

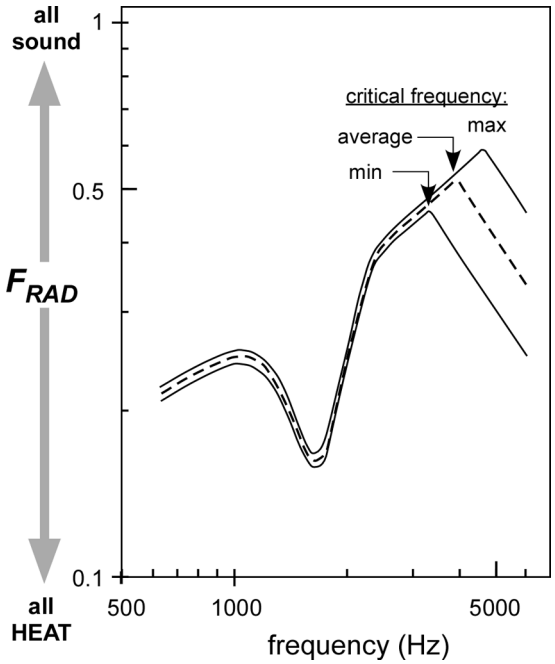

FIG. 7. Egress filter (mass-corrected) F_{RAD} for thick plates (min. $f_{crit} = 3.3$ kHz) graduated to average ($f_{crit} = 3.9$ kHz) and then thin (max. $f_{crit} = 4.6$ kHz).

mode frequencies in the form $f \propto f_{crit}^{-x}$, $x = 1$ for a flat plate, but for a shell $x < 1$. Such an f_{crit} "stretch" appears in Fig. 6 where f_2, f_5, f_{B1^-} and f_{B1^+} are plotted vs effective f_{crit} for nine violins with plate and corpus mode data. (The high predicted f_{crit} for mode #2 implies small effect on the *effective* f_{crit} estimate.)

Using the trend line equations from Fig. 6 to convert the 14-violin average $f_{crit} \approx 3.9$ kHz into B1 frequencies gave $f_{B1^-} \approx 470$ Hz, $f_{B1^+} \approx 543$ Hz, in good agreement with actual experimental averages of 470 and 541 Hz. Similarly, f_5 was predicted to be 349 Hz, compared to the average 352 Hz for the nine violins with known plate mode frequencies. Both results validate the trend line equations used. For the *Titian* Stradivari (1715) with $f_{crit} \approx 3650$ Hz but no plate mode frequencies, the trend line prediction $f_5 = 354$ Hz, can be compared to a top plate $f_5 = 360$ Hz for a 1713 Stradivari.[21] $B1^-$ and $B1^+$ trend line predictions of 476 and 552 Hz were close to the measured 472 and 546 Hz, respectively. The trend line equations of Fig. 6 are crucial to computations of the radiativity profile.

2. F_{RAD}

Figure 7 shows computed F_{RAD} results incorporating: (1) violin plate mass→M variations from empirical f_5→plate mass relationships[20] at three critical frequencies, viz., 3.3 kHz (minimum observed), 3.9 kHz, (14-violin average) and 4.6 kHz (maximum observed), and 2) an empirical "dimple" function to reproduce the experimentally observed dimple in R_{eff} near 1.6 kHz that carries over into ζ_{rad}. (Plates comprise nominally half of M.) The simplified F_{RAD} systematics show a clear "filter" effect strongly enhancing vibration-to-radiation conversion near f_{crit}.

[Although the violin has no obvious resemblance to simple geometric shapes, it does show characteristics *reminiscent* of the thin-walled cylinder or cylindrical shell, viz., (1) at the ring frequency f_{ring} (= longitudinal wave velocity/ circumference) for a thin-walled cylinder the modal density peaks and (2) above f_{ring} R_{eff} dips, rising finally to flat plate values near f_{crit},[22,23] both observed for the violin. Estimates of the violin's ring frequency fall near 1 kHz.[23] Until more definitive analysis emerges "ring" as used here remains only a convenient label.]

B. The Gatekeeper

In Eq. (9) $\frac{1}{2}M\langle Y(\omega)^2\rangle$ must incorporate all the dynamic effects related to: (1) changing the rocking frequency f_{rock} of the bridge (measured after clamping the bridge feet in a heavy vise), (2) the bridge-bridge island interface, (3) a modal density peak near 1 kHz, and (4) a body hill (BH) related to cutting the *f*-holes,[24] where extensional motion parallel to the bridge feet peaks and the bridge/bridge island impedance ratio reaches a minimum.[10] At present *none* of these effects has a reliable theoretical treatment.

In the statistical region above 630 Hz $\langle Y(\omega)^2\rangle$ will be replaced by our 14-violin, 250 Hz band-average mobility $\langle Y_{14}{}^2\rangle$, since all strongly radiating signature modes below 600 Hz are covered by the dual-Helmholtz model. Because all our simultaneous vibration-radiation measurements were for excitation at the bridge, we must in effect mathematically transform the original violin *excited-via-bridge* corpus mobility space to a *distributed*-excitation space—where no bridge intercedes between applied force and measured response—via a statistical mobility function to isolate-emphasize bridge filter effects.

1. Distributed-excitation statistical mobility

A statistical mobility function $Y_{stat}{}^2$ for *distributed* excitation requires averaging over a "large population of grossly

similar, but slightly different systems."[22] Treating all violins as being the "same" in this average reflects the scientific reality that easily *perceived* violin quality differences do not readily show themselves in such measurements. Y_{stat}^2 requires at least five modes per band, well satisfied by the 14-violin ensemble average in 250 Hz bands with a minimum 12 modes/band over the entire frequency range, and spatially uniform mass per unit area, attained only approximately for the spruce-maple substructures with densities ~400 to ~600 kg/m^3 and varying graduations. However, the normalization and simulations of *trends* minimize the effect of any such faults as only the general form of Y_{stat}^2 is needed. This mathematical transformation never loses the measured dynamical quantities inherent in $\frac{1}{2}M\langle Y_{14}^2\rangle$, choosing only to express them in a different mathematical form.

Since experimental mobility-radiativity in the 1375 Hz band was hardly affected by f_{rock} changes,[3] Y_{stat}^2—which has *no* bridge filter effects—was normalized to $\langle Y_{14}^2\rangle$—which does—at 1375 Hz, where both should coincide. With this normalization Y_{stat}^2 needs only modal density $n(f_c)$, computed over 250 Hz bands, the band-center frequency f_c, total damping $\zeta_{tot} \propto f^{-0.34}$ and M as variables,[22] i.e.,

$$Y_{stat}^2(f_c) \propto \frac{n(f_c)}{f_c \cdot \xi_{tot}(f_c) \cdot M^2}. \tag{10}$$

Updating an earlier published result[23] $n(f_c)$ was computed band-by-band up to 4 kHz for the 14-violin ensemble, and from 4 to 5 kHz for a 5-violin subset by counting all (non-string) modes in a band, not just those deemed strong enough to fit. (The lowest band covered only 300–500 Hz to exclude A0 from the B1$^-$ region, and A1 was dropped from the count.) Over their common range these $n(f_c)$ values were quite comparable to the vacuum-FEA results of Knott for a fully strung-up violin with sound post.[25] Our statistical "average" (good) violin had a minimum of ~2.2 modes/band, rising to a maximum $n(f_c) \approx 4.4$ modes/band near 1.1 kHz; $n(f_c)$ varied smoothly over this range and was well parameterized by a 6th order polynomial: $n(f) = -4.41 \times 10^{-21} f^6 + 1.18 \times 10^{-16} f^5 - 1.18 \times 10^{-12} f^4 + 5.71 \times 10^{-9} f^3 - 1.39 \times 10^{-5} f^2 + 1.54 \times 10^{-2} f - 2.18$. $\langle Y_{14}^2\rangle$ and Y_{stat}^2 (normalized at 1375 Hz) are shown in Fig. 8 (left).

Since Y_{stat}^2 was normalized to $\langle Y_{14}^2\rangle = 3.91 \times 10^{-4}$ m^2/N^2 *and* all 3-resonance fits required $\Phi = 1 \pm 0.01$ as a constraint at 1375 Hz, the gatekeeper filter retains this value at 1375 Hz throughout all calculations.

Surprisingly Y_{stat}^2 should not change appreciably on sound post removal—even though this dramatically degrades violin sound and causes significant changes in mode shapes,[13] implying significant changes in the bridge feet interaction with the corpus—because the damping *exponent* and $n(f_c)$ hardly change.

2. Isolating bridge filter effects

If we define a shape function $\Phi_{14} = \langle Y_{14}^2\rangle / Y_{stat}^2$, the gatekeeper now becomes

$$\frac{1}{2}M\langle Y_{14}^2(f)\rangle = \frac{\Phi(f) \cdot n(f)}{f_c \cdot \xi_{tot}(f) \cdot M}. \tag{11}$$

The combined behavior of $n(f)$, f and $\zeta_{tot}(f)$ creates a smooth, near-monotonic fall off in Eq. (11). Only Φ clearly displays the bridge-filter-related structure in $\langle Y_{14}^2\rangle$, hence it is labeled the "shape function." Applying the same procedure to the average bridge foot mobility $\langle Y_{bf}^2\rangle$ in the bridge waist trim experiment[3] creates Φ_{bf}, and reveals the bridge filter effects with even more clarity [Fig. 8(right) inset, $f_{rock} = 3.2$ kHz].

The highest frequency peak in Φ_{bf} tracked f_{rock} changes quite closely. This behavior was consistent with the bridge model calculations of Woodhouse.[26] Accordingly this feature was parameterized by the f_{rock}-dependent resonance function as shown in Fig. 8(right).

The two resonance-like structures in Φ_{bf} below the f_{rock} peak showed little dependence on f_{rock} or f_2 and f_5. These were labeled as a "ring" structure near 1 kHz and a BH structure near 2.3 kHz (following Jansson and collaborators). BH appears linked to the cutting of the slot-like *f*-holes,[24] a drastic mechanical modification in the very region most sensitive to bridge-corpus interaction. When "structures" such as these do not vary significantly with bridge or plate mode frequencies in the severely constrained environment of the dynamic filter model—absent physical model predictions—they must

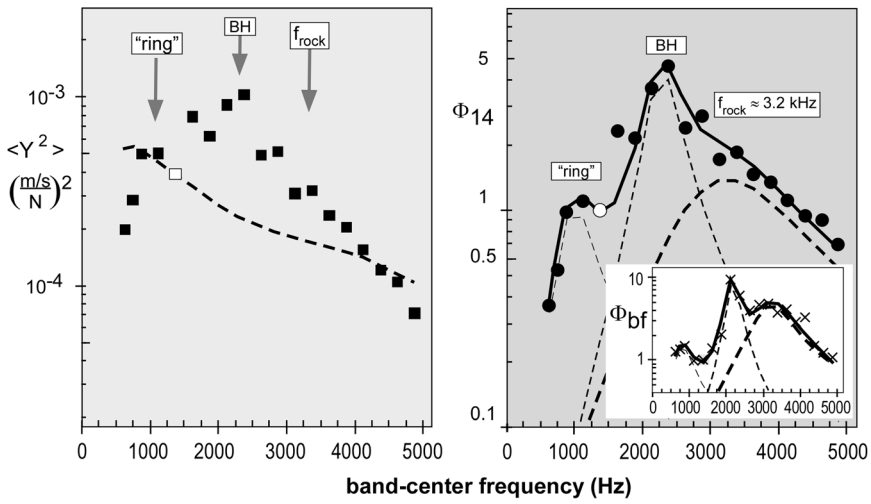

FIG. 8. The 250 Hz band averages: (left) $\langle Y_{14}^2\rangle$ (■) vs Y_{stat}^2 (- - -); 1375 Hz norm.; (right) 3-resonance parameterization of Φ_{14}, $f_{rock} \approx 3.2$ kHz, and (inset) Φ_{bf} for $f_{rock} = 3.2$ kHz. (individual resonances: - - -, sum (—)).

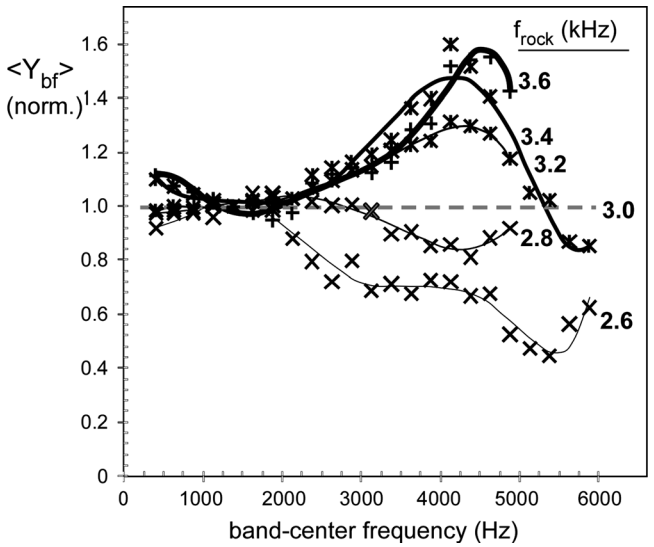

FIG. 9. $\langle Y_{bf}\rangle$ (norm. to 3.0 kHz data) for $f_{rock} = 2.6$ and 2.8 kHz (×); 3.2 and 3.4 kHz (✱), and 3.6 kHz (+) with 6th order polynomial fits.

be treated as experimentally determined "constants," here parameterized with two fixed-frequency resonance functions

Thus just three resonance functions—two fixed frequency, one variable—parameterize Φ_{bf} quite well. Applying the same 3-resonance parameterization to Φ_{14}, with "ring" and BH fixed in frequency and $f_{rock} \approx 3.2$ kHz, also gave good general overall agreement as shown in Fig. 8(right).

The shape function Φ_{14} can now be used for any violin with $f_{rock} \approx 3.2$ kHz. If f_{rock} is not known—the case for individual violins in the 14-violin ensemble—an additional parameterization scheme is needed to "scale" Φ_{14} to another f_{rock} for any particular violin (as was done for the Strad copy violin in Fig. 5). Again we turn to the Oberlin bridge experiment dataset where f_{rock} was varied from 2.6 to 3.6 kHz in 0.2 kHz steps to provide the systematics needed to compute the effect of f_{rock} changes.

3. Changing f_{rock}

We assume that ~50 milligram bridge *waist* trims off a ~2 g bridge on a ~400 g violin to drop f_{rock} from 3.6 to 2.6 kHz cannot have a significant effect on *corpus* mode frequencies, dampings or shapes. (The "inverse mute" effect of bridge wing-mass trims can be seen in Fig. 11 of Ref. 3.) Thus only Φ can change in Eq. (11) when changing f_{rock}, i.e., $\Phi \rightarrow \Phi'$ and $\langle Y^2\rangle \rightarrow \langle Y'^2\rangle$. Applying Eq. (11) for the new f_{rock} and dividing by the original f_{rock} Eq. (12) defines the scaling function $S(f)$,

$$S(f) = \frac{\Phi'}{\Phi} = \frac{\langle Y'^2\rangle}{\langle Y^2\rangle} = \frac{\langle Y'^2_{bf}\rangle}{\langle Y^2_{bf}\rangle}, \tag{12}$$

where Eq. (12) relies on the fact that for each mode the average bridge foot mobility $\langle Y_{bf}{}^2\rangle$ is a good *relative* measure of that mode's excitation and thus *in the ratio* can substitute for the average-over-corpus $\langle Y^2\rangle$. Hence the new shape function in Eq. (11) becomes $\Phi' = \Phi \cdot S(f)$ and,

$$\frac{1}{2} M\langle Y'^2_{14}(f)\rangle = \frac{\Phi(f)\cdot n(f)\cdot S(f)}{f_c \cdot \xi_{tot}(f)\cdot M}. \tag{13}$$

[When f_{rock} is unchanged $S(f) = 1$.]

Our $S(f)$ could be straightforwardly replaced by a similar scaling ratio from systematic theoretical calculations such as those by Woodhouse[26] (cf. Fig. 15) based on a bridge set on flat plates with no *f*-holes. Unfortunately, this model predicts scaling behavior *opposite to that seen experimentally* both by Jansson and Niewczyk[27] and in Fig. 9. Consequently experimental scaling functions have been retained.

Using the *fixed-violin/variable-bridge* dataset Fig. 9 presents the ratio $\langle Y_{bf}\rangle$ for each f_{rock} between 2.6 and 3.6 kHz divided by $\langle Y_{bf}\rangle$ at $f_{rock} = 3.0$ kHz. Figure 9 also includes 6th order polynomial fits used to parameterize each ratio (all $r > 0.97$). Each of these polynomials *squared* defines a function $F_{rock}(f; f_{rock})$ for each f_{rock} (see Table I). Hence

$$S(f) = \frac{F_{rock}(f; f'_{rock})}{F_{rock}(f; f_{rock})}, \tag{14}$$

where the prime is always for the *final* f_{rock}.

It is apparent from Fig. 9 that f_{rock} changes primarily affect the mobility profile near f_{rock}. The great diminution in $\langle Y_{bf}\rangle$ seen in this region as f_{rock} decreases was seen previously in 1999 by Jansson and Niewczyk,[27] who dropped f_{rock} to 1.5 kHz, far below our cautious limit for possible bridge waist failure in playing-listening tests.

The mid-frequency 1–2 kHz region was hardly affected by f_{rock} changes, with essentially no variation at 1375 Hz, our normalization point for $Y_{stat}{}^2$. Larger, but still small compared to the f_{rock} region, are the changes in the lowest two bands dominated by $B1^-$ and $B1^+$.

Signature mode bridge vibrations show nominally rigid body rocking behavior; near f_{rock} the bridge feet hardly move while the bridge top shows a complex "wiggle-rock."[3] Above about 5000 Hz bridge tuning effects appear to diminish.

TABLE I. F_{rock} polynomials (2600 Hz ≤ f_{rock} ≤ 3600 Hz).

f_{rock}	F_{rock} (fit range 400–5000 Hz, except as noted)
2600[a]	$[3.774\times10^{-21}f^6 - 6.618\times10^{-17}f^5 + 4.372\times10^{-13}f^4 - 1.338\times10^{-9}f^3 + 1.845\times10^{-6}f^2 - 9.856\times10^{-4}f + 1.102]^2$
2800	$[-6.492\times10^{-22}f^6 + 1.134\times10^{-17}f^5 - 6.637\times10^{-14}f^4 + 1.567\times10^{-10}f^3 - 1.535\times10^{-7}f^2 + 8.889\times10^{-5}f + 0.955]^2$
3000	1
3200	$[-2.010\times10^{-21}f^6 + 3.007\times10^{-17}f^5 - 1.819\times10^{-13}f^4 + 5.575\times10^{-10}f^3 - 8.545\times10^{-7}f^2 + 6.092\times10^{-4}f + 0.843]^2$
3400[a]	$[3.416\times10^{-21}f^6 - 5.679\times10^{-17}f^5 + 3.502\times10^{-13}f^4 - 1.020\times10^{-9}f^3 + 1.539\times10^{-6}f^2 - 1.191\times10^{-3}f + 1.399]^2$
3600	$[-9.279\times10^{-21}f^6 + 1.381\times10^{-16}f^5 - 7.962\times10^{-13}f^4 + 2.235\times10^{-9}f^3 - 3.059\times10^{-6}f^2 + 1.756\times10^{-3}f + 0.764]^2$

[a]Fit range 400–6000 Hz.

C. Statistical region dynamic filter equation

Combining the gatekeeper from Eq. (13) and egress from Eq. (9) and cancelling terms gives the ultimate form of the statistical region radiativity profile

$$\langle \mathrm{R}^2(\mathrm{f})\rangle \propto \frac{\Phi(\mathrm{f})\cdot n(\mathrm{f})\cdot S(\mathrm{f})}{\mathrm{M}} F_{RAD}(\mathrm{f}), \tag{15}$$

[A useful nominal value for Eq. (15) would be $\langle \mathrm{R}^2\rangle \approx 0.15$ $\mathrm{Pa}^2/\mathrm{N}^2$ (average violin) at $\mathrm{r}=1.2$ m and 1375 Hz, a value unaffected by $\mathrm{f}_{\mathrm{rock}}$ changes.]

In statistical terms modal density is the least variable term in Eq. (15), hardly affected by plate tuning or sound post removal. Plate tuning over the limited range of our experimental dataset could be expected to affect the shape function somewhat, as could the shape, size and placement of the *f*-holes in the "bridge island."

In the context of the dynamic filter model the egress filter is now just F_{RAD}, computed from the radiation-total damping ratio that collects all the damping—energy loss—properties of the violin into one dimensionless term. The gatekeeper in the statistical region depends on the product of the shape function, modal density, and scaling function, where $S(\mathrm{f})=1$ if bridge tuning is unchanged. To compute the statistical region skeleton radiativity profile for the well-known Strad copy violin in Fig. 5, F_{RAD} was computed for experimental $\mathrm{f}_{\mathrm{crit}} \approx 4.2$ kHz, while $\Phi(\mathrm{f})$ and $n(\mathrm{f})$ in Eq. (15) were taken directly from the 14-violin ensemble results with bad violin mass $\mathrm{M}=0.41$ kg. The only variable in Eq. (15) was $S(\mathrm{f})$. Varying F_{rock} (using functions in Table I) for the best overall fit gave $\mathrm{f}_{\mathrm{rock}} \approx 2.8$ kHz.

1. Statistical model general systematics

In 1946 Frederick Saunders summarized decades of research by remarking that eminent violinists looked for two main qualities in a violin: "first, great power, and second, an even distribution of strength among all ranges of frequency, the lowest octave being of special importance."[28] Does Eq. (15) offer any quantitative insights into the most general aspects of these judgments?

The "even distribution of strength" reflected in the relatively smooth radiativity profile of our three old-Italian violins vs three bad ones[10] was consistent with this summary statement. The BH was the highest radiativity peak for the bad and average (good) violin and its origin—likely from cutting *f*-holes—suggests examining the bridge feet-corpus interface, since bridge waist trims hardly affect it. (Typical maintenance-repairs on old violin top plates near the bridge feet could easily affect this interface.)

The desirable "great power" can be approached from a number of perspectives, including perceptual ones:

(1) *Maximize* F_{RAD}—violins need only minimize internal and support fixture damping to become more "powerful," yet too little damping has an adverse effect on violin sound.
(2) *Reduce total mass M*—unsurprising given Newton's 2nd Law. M for the three old Italian violins in our dataset was ~10% lower than for the bad violins.
(3) *Increase* $n(f_c)$—reduced plate mass reduces mode frequencies and their separation, thus increasing $n(\mathrm{f_c})$ *and* reducing M. But the drop in B1 frequencies points to more $\mathrm{R_{A0}}$ and a corresponding increase in $\mathrm{f_{crit}}$, implying a *relatively* weaker mid-frequency response overall.
(4) *Increase* $n(f_c)$—by adding small substructures whose modes are then subsumed into the whole. Possibly mode frequencies could add to $n(\mathrm{f_c})$ in or near a region where emphasis is desired? Of course added mass from small substructures that do not radiate effectively might divert string vibration energy to create no net advantage.
(5) *Psychoacoustics*—in an auditorium where typical reverberation boosts the low and rolls off the high frequencies, perhaps *concentrating* sound in the 2–4 kHz range where the ear's sensitivity is greatest via a convergence of $\mathrm{f_{rock}}$ and $\mathrm{f_{crit}}$ could provide audible perceptual dividends?

Desirable strength in the "lowest octave" tends to single out A0 and thus how well corpus motions excite it. Later simulations that combine the deterministic and statistical regions utilize Eq. (15) to provide important *trend* information on A0 excitation due to plate and bridge tuning using the empirical plate modes→B1 relationship.

D. Plate modes to B1 modes

Violinmakers have generally neglected the effect of ribs—normally chosen to satisfy esthetic or cosmetic concerns—on violin dynamics even though they certainly knew not to make them too thick or thin. Schelleng for example thought only their mass was important in his octet scaling.[6] Normally, gluing free plates to the ribs should dramatically alter their mode shapes due to major boundary condition changes. In the unruly context of violin research the happy coincidence of the B1 nodal line patterns resembling those of plate modes #2 and #5 flipping between top and back could not be ignored.

In 1996 Schleske demonstrated that tuning plates over a wide range of frequencies had a relatively small effect on B1 frequencies,[20] a result that seemingly undermined any rationale for plate tuning other than possibly manufacturing consistency, but did not keep violinmakers from tuning plates. However an unorthodox view—B1 bending mode stiffness was dominated by rib (not plate) stiffness common to both modes—led to a heuristic flat-plate model incorporating rib stiffness that maintained (actually required) orthotropic wood plates.[4] (The physical argument underlying the model, reduced to its essentials, was that bending a plate in a particular way reveals a certain stiffness, *irrespective of the frequency of bending*.)

Taking the rib stiffness contribution to the 1st corpus bending modes as the same for each B1 in the model implies that subtracting B1 frequencies, $\mathrm{f_{B1^+}}-\mathrm{f_{B1^-}}=\Delta\mathrm{B1}$, approximately cancels rib stiffness, leaving mainly plate stiffness parameterized by the plate mode frequency difference, $\mathrm{f_5}-\mathrm{f_2}=\Delta 52$, to dominate ΔB1, resulting in the empirical trend line equation $\Delta\mathrm{B1}=(0.034\cdot\Delta 52)^{2.38}$. Another simple trend line equation, $\mathrm{f_{B1^+}}/\mathrm{f_{B1^-}}=2.32\times10^{-3}\cdot\Delta\mathrm{B1}+0.988$,

was generated from f_{B1^+}/f_{B1^-} vs $\Delta B1$, with limits $f_{B1^+}/f_{B1^-} \rightarrow 1$ as $\Delta B1 \rightarrow 0$.

Since $f_{B1^-} = \Delta B1/(f_{B1^+}/f_{B1^-} - 1)$ and $f_{B1^+} = f_{B1^-} + \Delta B1$, both B1 frequencies can be predicted from f_2 and f_5, typically within $\pm 3\%$ for our dataset. Remaining inside the limits of our database, a simple mathematical chain exists to start anywhere in the chain, using $f_2, f_5 \leftrightarrow f_{B1}$ and $f_5 \leftrightarrow f_{crit}$, to simulate skeleton radiativity profiles for a certain f_{rock}.

V. DYNAMIC FILTER MODEL SIMULATIONS

These first skeleton radiativity profile simulations will be limited to the range of experimental parameters in the database, using only the minimum-average-maximum values for plate and bridge tuning.

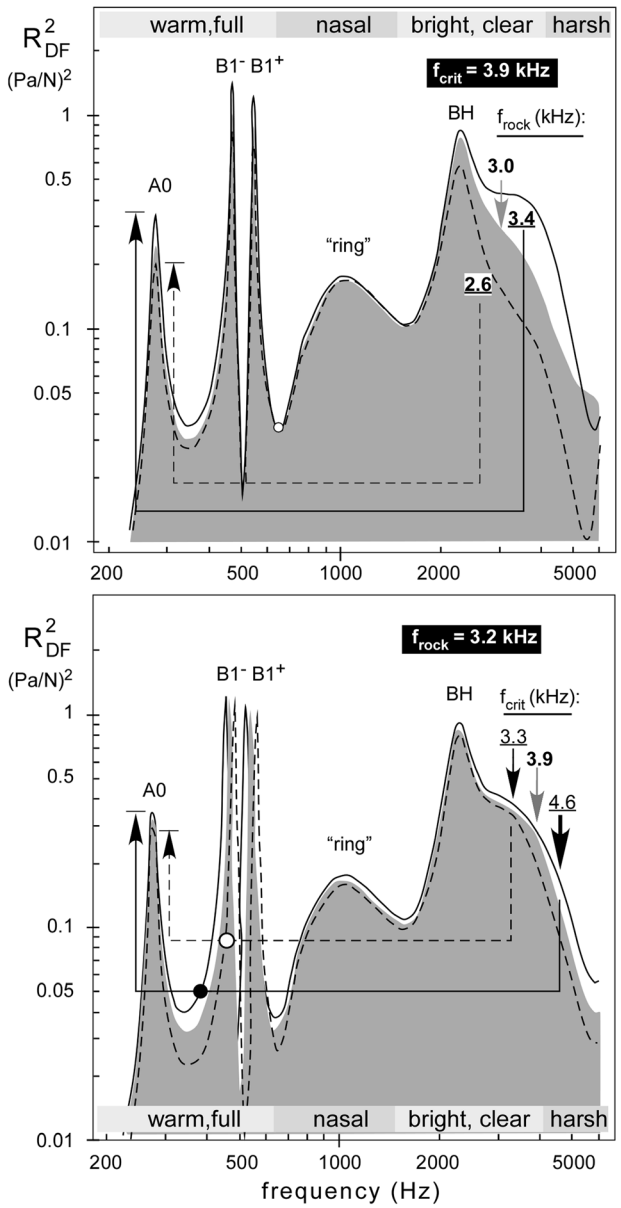

FIG. 10. Dynamic filter skeleton radiativity profile R_{DF}^2 (all same scale): (top) *fixed violin/variable bridge* $f_{crit} = 3.9$ kHz, f_{rock} stepped 2.6–3.0–3.4 kHz (f_{A0}, f_{B1^-}, f_{B1^+} VIOCADEAS averages). (bottom) Variable violin/fixed bridge for $f_{rock} = 3.2$ kHz, f_{crit} stepped 3.3–3.9–4.6 kHz. (Shaded curves represent average "good" violin starting results; arrows link f_{rock},f_{crit} changes to R_{A0}.)

All simulations used 14-violin-averages: 275 Hz, 2.5 %crit and 469 Hz, 1.0 %crit, for A0 and A1, resp. For B1: $f_{B1^-} = 470$ Hz, $\langle R_{B1^-} \rangle = 1.01$ Pa/N, $\zeta_{B1^-} = 1.22$ %crit; $f_{B1^+} = 541$ Hz, $\langle R_{B1^+} \rangle = 0.95$ Pa/N, $\zeta_{B1^+} = 1.15$ %crit.

A. Effect of bridge tuning on $\langle R^2(f) \rangle$: f_{crit} fixed

The effect of stepping f_{rock} from 2.6 to 3.0 to 3.4 kHz on the computed dynamic filter radiativity profile R_{DF}^2 was simulated for f_{crit} fixed at our average 3.9 kHz. Choosing a value for f_{crit} sets f_2, f_5, f_{B1^-}, f_{B1^+} using the mathematical chain developed earlier. Although our average f_{rock} was 3.2 kHz the *fixed f_{crit}/variable f_{rock}* simulations used an "average" $f_{rock} = 3.0$ kHz to take advantage of the 6 kHz maximum frequency for the 3.0, 2.6 and 3.4 kHz data sets. The 3.4 kHz simulation was also chosen rather than 3.6 kHz maximum f_{rock} because it had similar behavior and a wider frequency range. The effect of f_{rock} changes on the B1 modes was also incorporated into the dual-Helmholtz calculations for these simulations, with B1 radiativity changes mirroring those shown for A0.

The simulation results are shown in Fig. 10(top). Also note the introduction of "robust" qualitative descriptors "warm, full," "nasal," "bright, clear," and "harsh" for violin sound[29,30] superimposed on their respective frequency ranges in these plots. These terms serve as a guide to judge qualitative *trends in sound* related to *radiativity profile trends* as f_{rock} was varied.

B. Effect of plate tuning on $\langle R^2(f) \rangle$: f_{crit} changed

Changing f_{crit} is more complicated than changing f_{rock} since f_2, f_5, and f_{B1^-}, f_{B1^+} must also change. The f_{crit} choices, stepped from 3.3 to 3.9 to 4.6 kHz (our minimum, average, and maximum values, resp.) create the *fixed f_{rock}/variable f_{crit}* curves shown in Fig. 10(bottom) using the 14-violin gatekeeper filter from Eq. (13) and $f_{rock} \approx 3.2$ kHz.

Comparing curves for minimum-to-maximum f_{rock} with minimum-to-maximum f_{crit} it is apparent from Fig. 10 that the gatekeeper is a *much* stronger filter than the egress, and (b) the major effect of f_{rock} and f_{crit} lies above the BH peak between ~3 and ~5 kHz, falling where the ear is most sensitive.

VI. CONCLUSIONS

Violin acoustics suffers from limitations akin to the prisoners in Plato's allegory who see "reality" in the form of shadows cast by people and objects on the walls of the cave. We cannot capture the violinist's bone conduction+near-field ear, the tactile embrace of the instrument or the personal auditory processing system. Yet that is mostly irrelevant to this dynamic filter model, which asks—and provides somewhat imperfect answers to—only questions about how modifying plate mode and/or bridge rocking frequencies will affect the radiativity profile, thereby giving makers some sense of how each affects the sound.

The model exposes some of the seemingly conflicting underpinnings of plate-bridge tuning, viz., tuning plate modes at the low frequency end also affects the high frequency end of the radiativity profile through the link to the

critical frequency. Conversely tuning the bridge rocking mode at the high frequency end affects low frequency signature mode radiativity. Thus if the plates are a bit thick, raising the B1 frequencies and lowering f_{crit}, applying a "countervailing" bridge tuning—raised f_{rock}—might very well be able to compensate. Conversely, too-thin plates could be compensated for by lowering f_{rock}.

ACKNOWLEDGMENTS

The author wants to express appreciation for the systematic, careful modifications by violinmakers at the Oberlin Violin Acoustics Workshops that were essential to the model development. Although our debt to those who "fathered" the violin into close-to-its-present-day form has long been acknowledged, setup people who have labored in relative obscurity over centuries to maintain the excellence of legendary old violins are equally important, and may well be the real "Secret of Stradivari." All the rest of course is up to the violinist. The author wishes to acknowledge discussions with Frank Fahy and to thank the anonymous reviewers for many helpful criticisms and comments.

[1]L. Cremer, *The Physics of the Violin* (MIT Press, Cambridge, 1984), Chaps. 10 and 12.
[2]G. Bissinger, "Modal analysis of a violin octet," J. Acoust. Soc. Am. **113**, 2105–2113 (2003).
[3]G. Bissinger, "The violin bridge as filter," J. Acoust. Soc. Am. **120**, 482–491 (2006).
[4]G. Bissinger, "Surprising regularity between plate modes 2 and 5 and the B1 corpus modes: Part I," J. Violin Soc. Am. **21**, 85–103 (2007).
[5]C. M. Hutchins, A. S. Hopping, and F. A. Saunders, "Subharmonics and plate tap tones in violin acoustics," J. Acoust. Soc. Am. **31**, 1443–1449 (1960).
[6]J. C. Schelleng, "The violin as a circuit," J. Acoust. Soc. Am. **35**, 326–338 (1963); **35**, 1291(E) (1963).
[7]G. Weinreich, C. Holmes, and M. Mellody, "Air-wood coupling and the swiss-cheese violin," J. Acoust. Soc. Am. **108**, 2389–2402 (2000).
[8]C. M. Hutchins, "A study of the cavity resonances of a violin and their effects on its tone and playing qualities," J. Acoust. Soc. Am. **87**, 392–397 (1990).
[9]G. Weinreich, "Sound hole sum rule and the dipole moment of the violin," J. Acoust. Soc. Am. **77**, 710–718 (1985).
[10]G. Bissinger, "Structural acoustics of good and bad violins," J. Acoust. Soc. Am. **124**, 1764–1773 (2008).
[11]G. Bissinger, "Structural acoustics model of the violin radiativity profile," J. Acoust. Soc. Am. **124**, 4013–4023 (2008).
[12]H. Meinel, "On the frequency curves of violins," Akust. Z. **2**, 22–33 (1937).
[13]G. Bissinger, "Some mechanical and acoustical consequences of the violin soundpost," J. Acoust. Soc. Am. **97**, 3154–3164 (1995).
[14]G. Bissinger, E. G. Williams, and N. Valdivia, "Violin f-hole contribution to far-field radiation via patch near-field acoustical holography," J. Acoust. Soc. Am. **121**, 3899–3906 (2007).
[15]G. Weinreich, "Radiativity revisited: Theory and experiment ten years later," Proc. Stockholm Music. Acoust. Conf. 1993, Royal Swed. Acad. Mus. **79**, 432–437 (1994).
[16]O. Christensen and B. Vistisen, "Simple model for low-frequency guitar function," J. Acoust. Soc. Am. **68**, 758–766 (1980).
[17]E. A. G. Shaw, "Cavity resonance in the violin: Network representation and the effect of damped and undamped rib holes," J. Acoust. Soc. Am. **87**, 398–410 (1990).
[18]G. Bissinger, "A0 and A1 coupling, arching, rib height, and f-hole geometry dependence in the 2-degree-of-freedom network model of violin cavity modes," J. Acoust. Soc. Am. **104**, 3608–3615 (1998).
[19]*The Physics of Musical Instruments*, 2nd ed., edited by N. H. Fletcher and T. D. Rossing (Springer, New York, 1998), Chaps. 3 and 8.
[20]M. Schleske, "Eigenmodes of vibration in the working process of a violin," Catgut Acoust. Soc. J. **3**, 2–8 (1996).
[21]C. M. Hutchins, "Stradivarius plate tests," Catgut Acoust. Soc. Newsl., **37**, 30 (1982).
[22]F. Fahy and P. Gardonio, *Sound and Structural Vibration: Radiation, Transmission and Response*, 2nd ed. (Academic Press, New York, 2007), Chaps. 1–3.
[23]G. Bissinger, "A unified materials-normal mode approach to violin acoustics," Acust. Acta Acust. **91**, 214–228 (2005).
[24]F. Durup and E. Jansson, "The quest of the violin bridge-hill," Acust. Acta Acust. **91**, 206–213 (2005).
[25]G. A. Knott, "A modal analysis of the violin using MSC/NASTRAN and PATRAN," M.S thesis, Naval Postgraduate School, 1987. Reprinted in Res. Pap. Violin Acoust. 1975–1993, edited by C. M. Hutchins (Acoustical Society of America, Woodbury, NY, 1997).
[26]J. Woodhouse, "On the bridge-hill of the violin," Acustica **91**, 155–165 (2005).
[27]E. V. Jansson and B. K. Niewczyk, "On the acoustics of the violin: bridge or body hill," Catgut Acoust. Soc. J. **4**(7), 23–27 (1999).
[28]F. A. Saunders, "The mechanical action of instruments of the violin family," J. Acoust. Soc. Am. **17**, 169–186 (1946).
[29]H. Meinel, "Regarding the sound quality of violins and a scientific basis for violin construction," J. Acoust. Soc. Am. **29**, 817–822 (1957).
[30]H. Dünnwald, "Ein erweitertes verfahren zur objectiven bestimmung der klangqualität von violinen," Acustica **71**, 269–276 (1990); English version "Deduction of objective quality parameters on old and new violins," Catgut Acoust. Soc. J. **1**(7), 1–5 (1991).